Two-dimensional model of calcium waves reproduces the patterns observed in *Xenopus* oocytes

Steven Girard, Andreas Lückhoff, James Lechleiter, James Sneyd,* David Clapham
Department of Pharmacology, Mayo Clinic and Foundation, Rochester, Minnesota; and *Department of Biomathematics, UCLA School of Medicine, Los Angeles, California 90024-1766

ABSTRACT Biological excitability enables the rapid transmission of physiological signals over distance. Using confocal fluorescence microscopy, we previously reported circular, planar, and spiral waves of Ca^{2+} in *Xenopus laevis* oocytes that annihilated one another upon collision (1). We present experimental evidence that the excitable process underlying wave propagation depends on Ca^{2+} diffusion and does not require oscillations in inositol (1, 4, 5) trisphosphate (IP_3) concentration. Extending an existing ordinary differential equation (ODE) model of Ca^{2+} oscillations to two spatial dimensions, we develop a partial differential equation (PDE) model of Ca^{2+} excitability. The model assumes that cytosolic Ca^{2+} couples neighboring Ca^{2+} release sites. This simple PDE model qualitatively reproduces our experimental observations.

INTRODUCTION

The phosphatidylinositol (PI)-linked pathway is used by dozens of G protein-linked receptor systems to mobilize intracellular calcium (2). A rise in the intracellular free $[Ca^{2+}]$ is a pervasive biological signal hypothesized to encode biological information in its spatio-temporal pattern (3, 4). We recently demonstrated agonist-induced Ca^{2+} waves that organized into spiral-like patterns in *Xenopus laevis* oocytes (1). Propagating Ca^{2+} wavefronts of constant amplitude and the mutual annihilation of any two colliding Ca^{2+} wavefronts suggested there may be an excitable process underlying these phenomena (1).

Simplified models of the PI-linked cascade, represented as ordinary differential equations (ODE), have been presented to account for oscillatory changes in free cytosolic $[Ca^{2+}]$. Depending on whether they predict oscillating $[IP_3]$, these models may be categorized into two types. One example of the first class incorporates the positive feedback of Ca^{2+} on PLC activity, and necessitates oscillations of $[IP_3]$ (5). The second class of models does not require changing $[IP_3]$ and includes a Ca^{2+} induced Ca^{2+} release (CICR) model (6). CICR is used here to denote Ca^{2+} dependence of release but not to specify involvement of ryanodine over IP_3 receptors.

The purpose of this study was to mathematically model the Ca^{2+} mobilizing machinery as an excitable medium. We represented the Ca^{2+} kinetics with a preexisting CICR model of Ca^{2+} oscillations and provide experimental rationale for the choice of this model (6, 7). With parameter values that do not result in steady oscillations, the local kinetics of this model describe an excitable system, with cytosolic Ca^{2+} considered the excitation signal. Furthermore, we show that this ODE model is mathematically analogous to the FitzHugh-Nagumo equations, a well studied representation of a typical excitable medium. Assuming the Ca^{2+} in the IP_3-insensitive store does not diffuse, we constructed and numerically solved a two-dimensional PDE representation of CICR. All the experimental observations in *Xenopus* oocytes, including spiral waves, were qualitatively reproduced. It should be noted that an analogous model, with Ca^{2+} and IP_3 acting as co-agonists at the IP_3 receptor, fits within this same mathematical construct (8).

Address correspondence to David Clapham.

MATERIALS AND METHODS

Adult, female *Xenopus laevis* toads were purchased from Xenopus I (Ann Arbor, MI). Incubation media for the oocytes was L-15 media (Gibco Chemical Co., Grand Island, NY). Injection solution contained in mM: 96 NaCl, 2 KCl, 2 $MgCl_2$, 5 HEPES, 1 EGTA; pH was adjusted to 7.5, and the osmolality was 250 mosmol/liter. Ca^{2+} Green was purchased from Molecular Probes (Eugene, OR), and IP_3S_3 was purchased from New England Nuclear (Boston, MA).

Ovarian lobes were removed under sterile conditions from anesthetized toads followed by immediate suturing of the incision. Stage V-VI oocytes were manually defolliculated, allowed to recover for at least 30 min, and were then injected with 50 nl of 20 μM IP_3S_3 ($\approx$1 μM final) and 50 nl of 0.25 mM Ca^{2+} Green ($\approx$12.5 μM intracellular concentration) while bathed in the Ca^{2+}-free injection solution. The IP_3S_3, stored as an ethanol solution, was lyophilized and redissolved in an equal volume of low Ca^{2+} water ($\approx$50 nM) immediately before use. To minimize Ca^{2+} entry, the oocytes were kept in the injection solution for 1–2 min after the injections.

Images (128 × 128 pixels) were taken on a Bio-Rad MRC 600 scanner (Cambridge, MA) adapted to an IM35 Zeiss microscope (Carl Zeiss, Inc., Thornwood, NY) using a 10× UV Planapo Olympus Objective (0.4 numerical aperture [N.A.]). With the PMT detector

aperture wide open (7 mm) to maximize the fluorescence signal, the size of the confocal section was 740 × 740 × 40 μm. An argon laser rated at 25 mW (Ion Laser Technology, Salt Lake City, UT) gave excitation at 488 nm, and a filter set was used to record fluorescence emission wavelengths greater than 510 nm. With the photomultiplier (PMT) gain maximized, neutral density filters were inserted in the excitation path to minimize photobleaching. The optical section giving the maximum fluorescence signal was selected and sequential images were collected at 1 Hz, digitized to 8 bits (255 greyscale values) and stored on a Nimbus VX personal computer (Research Machines Ltd., Oxford, UK) (Intel 80386 processor). A Silicon Graphics Personal IRIS system with ANALYZE software (Mayo Foundation, Rochester MN) was used to process the images.

Experimental section

Experiments with the poorly-metabolized analogue of IP_3, myo-inositol (1, 4, 5) trisphosphorothioate (IP_3S_3), suggested that spatiotemporal changes in the [IP_3] were not required for Ca^{2+} wave propagation. Fig. 1 *A* shows two oscillatory foci of Ca^{2+} that arose 3 min after IP_3S_3 injection and triggered the formation of Ca^{2+} waves that annihilated each other upon collision. Fig. 2 *A* is a still frame image of a spiral wave of Ca^{2+} release also triggered by ≈ 1μM IP_3S_3. IP_3S_3 was considered stable for the duration of these experiments and was assumed to compete for occupancy of the IP_3 receptor (9, 10, 11). Ca^{2+} efflux measurements in Swiss 3T3 cells showed that IP_3 was ~3.5 times more potent than IP_3S_3 (EC_{50} = 2.5 μM for IP_3S_3) (11). The organization of Ca^{2+} waves into spiral patterns, itself, also suggested local cooperativity rather than amplification of PLC by Ca^{2+}. Assuming PLC is located at the plasma membrane, the latter hypothesis would require PLC amplification and Ca^{2+} release from endoplasmic reticulum to behave in a spatially-concerted fashion. Because we observed spiral activity frequently (up to 30% in some studies), it seemed more likely that Ca^{2+} directly mediated the release of Ca^{2+} from intracellular stores. Also, the period of the spiral waves (5.5–10 s) was too brief to allow complete metabolism of IP_3 between successive wavefronts, given an estimated IP_3 half-life of 4 s (12). Additional data which rule out IP_3 as the propagating species are from our previous experiments

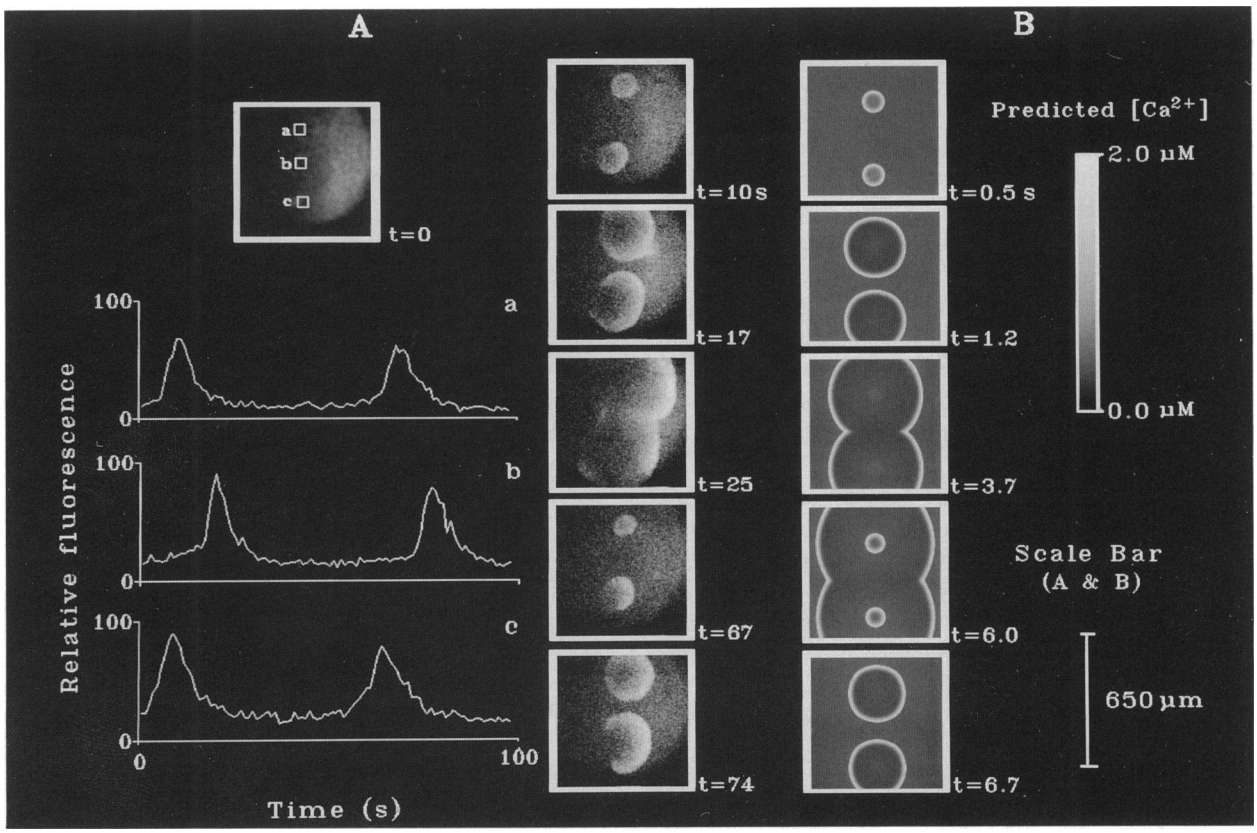

FIGURE 1 Pulsing foci of Ca^{2+} release. (*A*) Pulsing foci of Ca^{2+} release in a *Xenopus* oocyte were observed with confocal fluorescence microscopy 2–3 min after the injection of IP_3S_3 (≈ 1 μM final). Circular Ca^{2+} wavefronts originating from these foci propagated at speeds of ~26 μm/s (1). This figure shows two pulsing foci, each with a period of ~57 s between transients, and demonstrates the annihilation of colliding wavefronts. Five unfiltered, still frames of a single 760 × 760 × 40 μm confocal section are shown in the right column. For contrast, the greyscale from 32–71 has been expanded to cover the entire 255 (8 bit) range. The amplitude of similar Ca^{2+} waves were previously estimated to be 50–100 nM (1). Three (50 × 50 μm) regional Ca^{2+} Green fluorescence averages are plotted versus time in *a*, *b*, and *c*. (*B*) PDE model exhibits waves originating from oscillatory foci that annihilate upon collision. The following kinetic parameters were used: V_m = 455 μM/s, K_c = 0.9 μM, K_I = 2 μM, V_p = 65, K_p = 1, K_{leak} = 10, K_{ER} = 1. With the exception of the two circular regions discussed in the text, ν_o = 3.1. The entire grid was initialized to the steady-state values for these parameters. Five images of the predicted cytosolic [Ca^{2+}] are presented, corresponding to 0.5, 1.2, 3.7, 6.0, and 6.7 s.

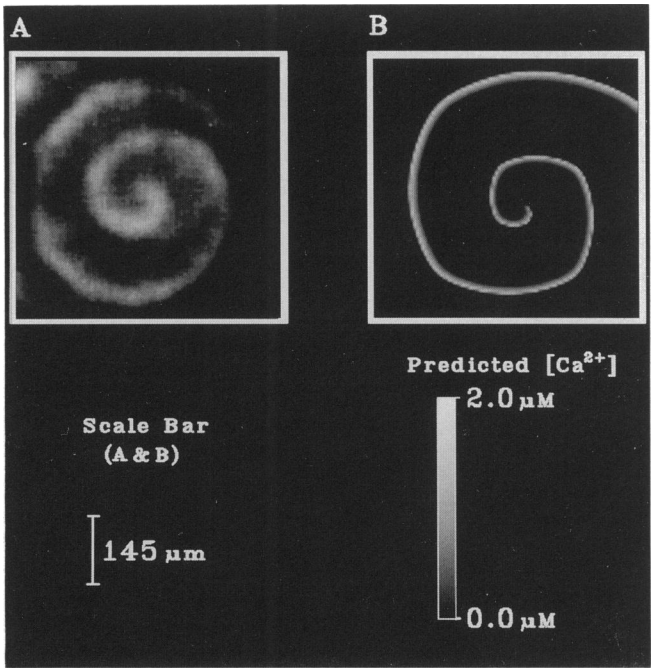

FIGURE 2 Spiral Waves of Ca^{2+} mobilization observed in *Xenopus laevis* oocytes and as a solution to the PDE model. (*A*) After injection of IP_3S_3, Ca^{2+} wave propagation in some oocytes was partially blocked by "refractory" regions, causing bending of the wavefronts and subsequent spiral-like behavior. These spirals were stable for up to 8 rotations, after which, they broke up into more disorganized patterns. The spiral wave in this figure had a wavelength (λ) of 135 μm, a period (T) of 5.5 s, and completed 6 revolutions in 33 s. (*B*) Still-frame image of the numerical solution to the two dimensional PDE model of CICR using the parameters in the legend to Fig. 1 *B*. The diffusion coefficient for cytosolic calcium was taken as 210 $\mu m^2/s$. The mesh was kinetically homogeneous and spirals were generated by altering the initial conditions as discussed in the text.

with *Xenopus* oocytes expressing exogenous muscarinic receptors (1). The diffusion coefficient (D) of the excitatory signal was measured to be 210 ± 80 $\mu m^2/s$ at 22°C, closer to estimates in other cells of the apparent diffusivity of Ca^{2+} (400–600 $\mu m^2/s$) than to estimates for IP_3 (33 $\mu m^2/s$) (13, 14). However, the effective diffusivity of Ca^{2+}, a function of the affinity, capacity, and mobility of Ca^{2+} buffers, has not been measured in the oocyte (15). Our data suggest that the excitatory signal is not IP_3, but do not prove that Ca^{2+} is the propagating species. Consequently, we postulated that $[IP_3]$ need not vary over time and space to generate complex spatio-temporal patterns of Ca^{2+} release, an important distinction that allowed us to rule out Ca^{2+} wave models that necessitate oscillating levels of $[IP_3]$.

THEORETICAL SECTION

ODE model of calcium transients

Given the data summarized above, we used a mathematical model of Ca^{2+}-induced Ca^{2+} release (CICR) proposed by Kuba et al. (16) and extended by Goldbeter et al. (6, 7) (Fig. 3). This model assumes two functionally distinct Ca^{2+} stores: a Ca^{2+}-sensitive store and an IP_3-sensitive store. Receptor occupancy leads to a constant $[IP_3]$ which, in turn, generates a steady flux of Ca^{2+} into the cytosol from the IP_3-sensitive Ca^{2+} stores. If the cytosolic $[Ca^{2+}]_c$ reaches a particular threshold, while the IP_3-insensitive Ca^{2+} store is sufficiently full, a rapid release of Ca^{2+} occurs through the calcium-sensitive channel. This model has two dependent variables: the cytosolic free $[Ca^{2+}]$ represented by c and the effective luminal $[Ca^{2+}]$ represented by l. The CICR rate (r_{CICR}) is taken from enzyme kinetics as the product of two fractional driving functions and the maximal rate of Ca^{2+} release, V_m. The first function of c has a Hill coefficient of 4 and an EC_{50} described by K_c; the second, a function of l, has a Hill coefficient of 2 and an EC_{50} of K_L. Because r_{CICR} is an increasing function of both c and l, a decrease in l terminates the release of Ca^{2+} from IP_3-insensitive stores in this model. Activation or inactivation processes of the calcium-sensitive channel are neglected. The rate of Ca^{2+} pumping into the Ca^{2+}-sensitive pool (r_{pump}) is taken as a saturable (V_p) function of c, with a Hill coefficient of 2 and an EC_{50} of K_p. The rate of Ca^{2+} leak out of the Ca^{2+}-sensitive pool ($r_{ER\ leak}$) is the product of K_{ER} and l. Similarly, the rate of Ca^{2+} extrusion out of the cell ($r_{extrusion}$) is assumed to be the product of K_{leak} and c.

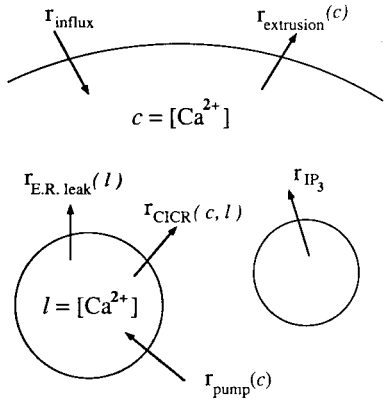

FIGURE 3 Schematic of the Ca^{2+} fluxes of the CICR model. The dependent variables of the model are l, the $[Ca^{2+}]$ in the lumen of the IP_3-insensitive Ca^{2+} stores with respect to the cytosolic volume, and c, the free cytosolic $[Ca^{2+}]$. The Ca^{2+} fluxes ($\mu M/s$) are represented by arrows and include: r_{CICR}, the rate of Ca^{2+} released from the IP_3-insensitive Ca^{2+} pool into the cytosol by CICR; r_{IP_3}, the net flux of Ca^{2+} from the IP_3-sensitive Ca^{2+} pool; r_{pump}, the rate of Ca^{2+} sequestration into the IP_3-insensitive store; $r_{ER\ leak}$, the nonspecific leak rate of Ca^{2+} from the IP_3-insensitive pool down its concentration gradient to the cytosol; $r_{extrusion}$, the rate of Ca^{2+} removal across the plasma membrane; and r_{influx}, the rate of Ca^{2+} influx across the plasma membrane. These fluxes are expressed mathematically in Eqs. 1 and 2 of the text.

The influx across the plasma membrane (r_{influx}) and the rate of release from IP_3-sensitive stores (r_{IP_3}) are constants in this model ($v_0 = r_{influx} + r_{IP_3}$). Thus, Eq. 1 represents the local rate of change of c as the net sum of Ca^{2+} fluxes into the cytosol (R_c). Similarly, Eq. 2 represents the net accumulation of Ca^{2+} into the IP_3-insensitive Ca^{2+} store, (R_l).

$$\frac{dc}{dt} = R_c(c, l) = v_0 + V_m\left(\frac{c^4}{c^4 + K_c^4}\right)\left(\frac{l^2}{l^2 + K_l^2}\right) - V_p\left(\frac{c^2}{c^2 + K_p^2}\right) + K_{ER}l - K_{leak}c \quad (1)$$

$$\frac{dl}{dt} = R_l(c, l) = V_p\left(\frac{c^2}{c^2 + K_p^2}\right) - V_m\left(\frac{c^4}{c^4 + K_c^4}\right)\left(\frac{l^2}{l^2 + K_l^2}\right) - K_{ER}l. \quad (2)$$

To investigate the kinetics of the model, we used a fourth-order Runge-Kutta algorithm to integrate Eqs. 1 and 2. Starting with parameters used by Goldbeter et al. (6), we decreased V_m from 500 to 455 μM/s and considered ($r_{IP_3} + r_{influx} = v_0$) as a bifurcation parameter because it was assumed to vary with agonist stimulation. Goldbeter et al. (6, 7) demonstrated periodic solutions to this model and showed that the frequency of oscillations varied over a particular range of v_0. In Fig. 4, *A* and *B* we set v_0 = 3.0 μM/s, and this resulted in a unique steady-state solution to the ODE model (c_{ss} = 0.31 μM and l_{ss} = 2.26 μM) (SS = steady-state) with no oscillations. Fig. 4 *A* represents a subthreshold stimulation (c_i = 0.32 μM and $l_i = l_{ss}$), after which the system relaxes directly to its steady-state. For the suprathreshold stimulation (c_i = 0.34 μM, $l_i = l_{ss}$) in Fig. 4 *B*, the steady-state is approached after an additional rapid, transient increase in c. Thus, a threshold concentration of cytosolic [Ca^{2+}] is required for excitation. For v_0 = 3.2 μM/s, oscillatory behavior was evident as shown in Fig. 4, *C* and *D*. The latent period to the first oscillation depends on the initial conditions (c_i, l_i), but the period between transients was independent of these initial values. For instance, Fig. 4 *D* represents a large stimulus to this oscillatory system (c_i = 0.5 μM), and this causes a rapid initiation of oscillations. Fig. 4 *C* demonstrates a delay to the onset of oscillations for minimal stimulation (c_i = 0.2 μM).

Fig. 5 shows the individual Ca^{2+} fluxes for the excitatory excursion in Fig. 4 *B*. The initial rapid increase in c was caused by CICR, which terminates when the IP_3-insensitive store is functionally depleted, or when l decreases far below K_l. The Ca^{2+} pump rate peaks and both r_{CICR} and r_{pump} then decline to steady-state over time. For these parameters, r_{IP_3}, r_{influx}, and $r_{ER\ leak}$ are minor Ca^{2+} fluxes in comparison to r_{CICR} and r_{pump}.

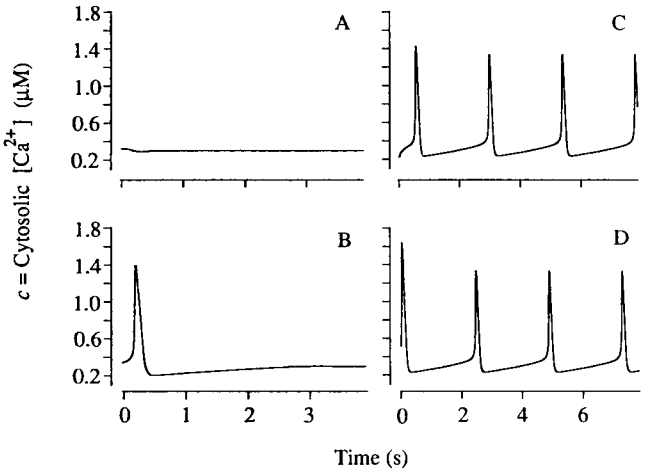

FIGURE 4 Threshold for excitation is predicted by CICR model. Plots of the cytosolic [Ca^{2+}] versus time for various c_i and v_0 values. The ODE model was numerically integrated with a fourth-order Runge-Kutta algorithm using a time step of 2 ms. (*A*) A subthreshold stimulation (c_i = 0.32 μM) results from the following parameters: V_m = 455 μM/s, K_c = 0.9 μM, K_l = 2 μM, V_p = 65 μM/s, K_p = 1 μM, $K_{extrusion}$ = 10 s^{-1}, K_{ER} = 1 s^{-1}, and v_0 = 3.0 μM/s. Given these parameters, there exists a unique, stable steady-state (c_{ss} = 0.31 μM, l_{ss} = 2.15 μM); l_i was set equal to l_{ss}. (*B*) A suprathreshold simulation (c_i = 0.34 μM), using the same parameters in *A*, results in a single excitatory excursion away from the steady-state. (*C* and *D*) Oscillatory solutions for v_0 = 3.2 μM/s, with all other kinetic parameters given in *A*. Plot *D* represents a large stimulus to the system (c_i = 0.5 μM) which causes the rapid initiation of oscillations. A minor stimulation (c_i = 0.2 μM) shown in plot *C*, results in oscillations having the same period and amplitude but with a longer latent period to the first oscillation.

Two dimensional model

An excitable medium may be defined as a collection of locally excitable processes linked by the diffusion of an excitatory signal (17). The diffusion coefficient of excitatory species triggering Ca^{2+} wave propagation in the *Xenopus* oocyte (*D*) was consistent with previous estimations of $D_{Ca^{2+}}$ in other cells. Therefore, we linked the locally-excitable processes given by Eqs. 1 and 2 by the molecular diffusion of cytosolic free Ca^{2+}, and set D_c to the measured value of 210 $\mu m^2/s$ (1). Assuming the luminal Ca^{2+} does not diffuse, the continuity equations for c and l, can be given as

$$\frac{\partial c}{\partial t} = D_c\left(\frac{\partial^2 c}{\partial x^2} + \frac{\partial^2 c}{\partial y^2}\right) + R_c(c, l) \quad (3)$$

$$\frac{\partial l}{\partial t} = R_l(c, l) \quad (4)$$

for cytosolic and luminal Ca^{2+}, respectively (18). Eq. 3, for example, represents a balance on cytosolic Ca^{2+}; the local accumulation ($\partial c/\partial t$) is equated to the sum of the

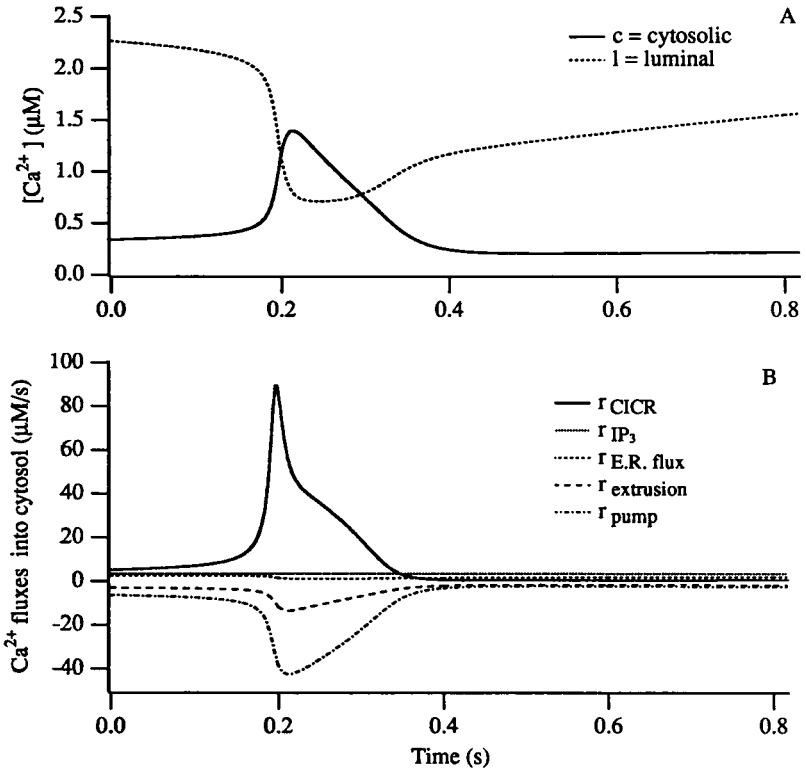

FIGURE 5 Individual Ca^{2+} fluxes contributing to a calcium transient. (*A*) The excitatory excursion in cytosolic and luminal $[Ca^{2+}]$ is shown with the individual Ca^{2+} fluxes below in *B*. A fourth-order Runge-Kutta algorithm was used to integrate Eqs. 5 and 6 with a time step of 1.0 ms. The parameters used are given in the legend to Fig. 1 *B* with the initial conditions $c_i = 0.38$ μM and $l_i = 2.15$ μM.

net flux into the cytosol, $R_c(c, l)$, and the rate of diffusion from neighboring regions. The second-order Laplacian term in Eq. 3 represents Fick's Second Law of molecular diffusion (18).

Computational methods

Because no analytical solution of Eqs. 3 and 4 was readily available, a computer program was developed to numerically integrate these coupled PDEs using a first-order forward Euler method (program is available upon request). The Laplacian term in Eq. 3 was approximated by averaging c over the nearest 4 mesh points (19). We used a grid dimension of 5.8 μm to facilitate direct comparison to the experimentally-acquired images. The time step was chosen to be 2.5 ms to insure numerical stability and convergence. The program read the kinetic parameters and the initial values (c_i, l_i) from text files and calculated the new values (c, l) for every mesh point forward in time (a 128 × 128 grid required 0.6 s per time step). It displayed the mesh graphically in pseudo-color and stored the data as image files after digitization to 8 bits. These image files were imported to the ANALYZE software package for further study. The computer program was written in C for the UNIX environment with modules adjusted to the graphic facilities of the Silicon Graphics Personal IRIS system.

Numerical results

A given mesh point could be initialized to one of three different "states" (refractory, excited, steady-state) for parameters that allowed a steady-state solution to the coupled ODEs given by Eqs. 1 and 2. If the dependent variables c_i and l_i were set to the steady-state values, the point was considered initially "stable." A "refractory" initial condition, which would not immediately support excitatory behavior, was created for some grid points by decreasing l_i from l_{ss} and/or by lowering c_i below c_{ss}. Conversely, an "excited" grid point was initialized by increasing c_i above the threshold value, as demonstrated in Fig. 4.

Pulsing Ca^{2+} foci represent two-dimensional chemical oscillators. To reproduce this behavior in a grid initialized to the "stable" values of c_{ss} and l_{ss}, we increased v_o from 3.1 to 3.38 μMs^{-1} in two circular regions of the grid. The circles had a radii of 53 μm (9 grid units) and were centered at grid coordinates (64,15) and (64,103) with

respect to the lower left-hand corner. Fig. 1 *B* shows that these regions of increased ν_0 behaved as pulsing foci (periods ~5.5 s) and initiated circular wavefronts (velocity ~100 μm/s) that mutually annihilated one another upon collision. Similar qualitative behavior is evident in the experimental data shown in Fig. 1 *A*.

The model spiral shown in Fig. 2 *B* was generated with the parameter set given in the Fig. 1 legend with the following initial conditions: (*a*) a 64 by 64 "excited" region in the lower left-hand corner with c_i = 1 μM and $l_i = l_{ss}$; (*b*) a 65 by 128 "refractory" region on the right half of the mesh with c_i = 0.2 μM and l_i = 0.8 μM. The rest of the grid was initialized to c_{ss} and l_{ss}. The wavelength (λ) of the experimental spiral was 135 μm and its period (T) was 5.5 s, completing 6 revolutions in 33 s. The model spiral in Fig. 2 *B* had a λ = 148 μm and T = 1.3 s. In general, the necessary feature for spiral wave initiation appeared to be the "rupture" or sharp bending of a wavefront. This wavefront bending was caused by a decrease in propagation speed within "refractory" regions; for these parameters, the refractory zone had a minimum diameter on the order of 100 μm for spiral initiation.

Because the velocities of the model spirals ($v = \lambda/T$) consistently exceeded the observed spiral velocities, D_c was studied parametrically. Fig. 6 shows that v is approximately linear for D_c between 50 and 800 μm²/s, with a slope of 0.28 ± .02 (R = .998). The other parameters and initial conditions are given in the Fig. 1 legend. With these initial conditions, no spiral waves were observed for D_c less than 50 μm²/s.

DISCUSSION

We have developed a two-dimensional representation of Ca^{2+} wave propagation in *Xenopus* oocytes by extending a preexisting ODE model of CICR-induced oscillations.

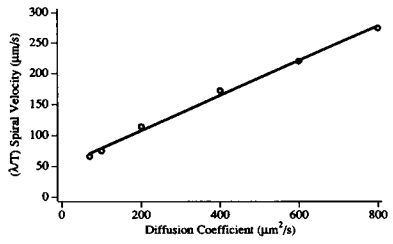

FIGURE 6 Spiral wave velocity as a function of D_c. The initial conditions used to generate spiral waves are given the text. The remaining kinetic parameters are listed in the legend to Fig. 1 *B*. The linear least squares best fit of v versus D is plotted along with the data points from numerical trials, represented as open circles (R = 0.997).

Our PDE representation of the release process predicted the following experimentally-observed phenomena: propagating, circular Ca^{2+} wavefronts of constant amplitude that initiate from oscillatory foci; mutual annihilation of colliding Ca^{2+} waves of any type; and organization into spiral Ca^{2+} waves. These results support the notion that CICR can account for these phenomena in the *Xenopus* oocyte, but they do not rule out other models of wave propagation. More specifically, we have demonstrated that the most likely positive feedback step is the action of Ca^{2+} at a local store, but we have not fully characterized this store. Preliminary experiments with caffeine suggest that *Xenopus* oocytes do, indeed, have distinct Ca^{2+} pools, a prerequisite for CICR. However, recent evidence from isolated rat brain microsomes suggests that Ca^{2+} acts as a coagonist with IP_3 at the IP_3 receptor (8). A mathematical representation of this coagonist model, assuming constant [IP_3] stimulation, would be analogous to the model presented here.

With the appropriate parameters, this CICR model predicts an activation threshold of cytosolic $[Ca^{2+}]_c$, below which the solution relaxes to a single steady-state (Fig. 4 *A*). Conversely, with a suprathreshold stimulus, it predicts a large, but transient increase in $[Ca^{2+}]_c$ (Fig. 4 *B*). Such an excursion, in the direction of an initial perturbation, is one characteristic of an excitable process (17). Furthermore, the model can be shown to be mathematically analogous to the FitzHugh-Nagumo equations, a well studied representation of many excitable media (see Appendix) (20, 21).

The experimentally-observed pulsing Ca^{2+} foci suggested that either the signal to release Ca^{2+} is spatially-restricted, or, alternatively, that the Ca^{2+} release mechanisms are heterogeneously distributed. IP_3S_3, which was assumed to diffuse evenly throughout the cytosol after intracellular injection, gave rise to focal Ca^{2+} transients that persisted for minutes. Assuming an even distribution of IP_3S_3, these data suggest that the Ca^{2+} release mechanisms of the *Xenopus* oocyte are spatially heterogeneous. Therefore, to produce pulsing foci, we increased the bifurcation parameter ν_0 in circular regions of the grid. Indeed, these sites gave rise to oscillatory, local increases in [Ca^{2+}] that subsequently triggered circular wavefronts (Fig. 1 *B*). Thus, the excitatory event underlying wave propagation may, in theory, be involved in the generation of pulsing Ca^{2+} foci.

Given a spatially-heterogeneous initialization of a grid with otherwise uniform kinetic parameters, the PDE model predicts complex patterns of Ca^{2+} wave propagation, including the organization into spiral waves. In numerical simulations, spiral wave initiation required the abrupt bending or "rupture" of a Ca^{2+} wavefront, as previously reported for models of other excitable media

(22–24). Likewise, experimental spirals originated when Ca^{2+} foci created neighboring refractory and excited regions. Therefore, this simple model accounts for the organization into spiral wave patterns; and conditions that were necessary for the initiation of simulated spiral waves mimic those we experimentally observed.

It is theoretically possible to obtain complex Ca^{2+} waves (pulsing targets and spiral waves) in two distinct manners. First, travelling waves may result from linking Ca^{2+} oscillators by diffusion, and these oscillations may be the result of negative feedback, positive feedback, or both. For complex waves to exist in an oscillatory system, the entire medium must be described by homogeneous kinetic equations. The second general mechanism to generate travelling waves is within an excitable medium. These waves are not generated by linking oscillators by diffusion, rather they are the result of perturbation of an excitable system that supports waves of excitation (16). In the CICR model, a local region, if given sufficient stimulus from its neighbors, reaches a threshold cytosolic $[Ca^{2+}]$ that triggers a rapid release of Ca^{2+} from internal stores. This excitability was observed by decreasing the bifurcation parameter (v_0) below the value that was necessary for periodic, or oscillatory solutions. In general, excitable media are more robust than linked oscillators and they provide a more attractive model for our experimental observations than linked oscillators.

It has been proposed that a given excitable medium has a unique spiral solution (i.e., a unique λ and T), with only the phase and spatial location of the spiral set by the initial conditions (17). The PDE model of CICR also seems to follow this rule because similar spiral waves were predicted under widely varying initial conditions. However, this PDE representation of CICR is a simple model and, as such, is limited by its assumptions. For example, the model uses a luminal calcium concentration (l) as a dependent variable because oscillations in cytosolic calcium concentrations necessitate changes in the concentration of Ca^{2+} in other compartments over time. Although buffers have been located in Ca^{2+}-sequestering organelles, the free $[Ca^{2+}]$ in the lumen of these stores is not known. Therefore, l represents a functional luminal Ca^{2+} concentration with respect to the cytosolic volume. The capacity of the store was taken as the maximal amplitude of a $[Ca^{2+}]_c$ transient, and was ~ 2 μM for the parameters we used. Although it is likely that the rate of CICR is a function of the $[Ca^{2+}]$ of an intracellular store, the inferred variable, l, may not correctly represent this relationship.

The Ca^{2+} wave propagation velocity was consistently higher than the velocity of experimentally-observed Ca^{2+} waves, and the many assumptions used to construct the PDE model possibly contributed to this discrepancy. Primarily, the kinetics of Ca^{2+} release and sequestration are not known in the oocyte, and future attempts to quantitatively model wave propagation need to address this issue. Also, restricting Ca^{2+} diffusion to two dimensions will necessarily increase the Ca^{2+} wave speed because molecular diffusion clearly occurs in all three spatial dimensions. Furthermore, r_{CICR} was assumed to be a continuous function of l and c, and ignored any activation or inactivation kinetics. If the CICR channel has relatively slow activation kinetics, this assumption would also lead to an overestimate of the Ca^{2+} wave velocity. Finally, limitation of Ca^{2+} diffusion in the cytosol by buffering would also significantly decrease the speed of propagation. To approximate buffering of Ca^{2+} in the PDE model, the effective diffusion coefficient of Ca^{2+} (D_c in the model) was decreased from its value in dilute aqueous solution (25, 26). Functionally, the PDE model spiral wave velocity (v) was found to be linear for D_c between 60–800 $\mu m^2/s$ with a slope of 0.28 μm^{-1} (Fig. 6).

The reported diffusivity of the excitatory species in *Xenopus* Ca^{2+} waves (210 $\mu m^2/s$) was used in the simulations and additional theoretical arguments provided a check of D_c (16). For a spiral with a velocity v defined as λ/T, the dimensionless quantity $(v\lambda/D_c)$ should be between 6π and $8\pi^2$, and is usually closer to $8\pi^2$ (17). For the experimental spiral, in this dimensionless number was 16, and for the model spiral, 79 (Fig. 2). Indeed, the measured D_c was higher than is theoretically expected for a spiral wave in a generic excitable medium with $\lambda = 135$ μm and a $T = 5.5$ s. In addition to the assumptions of the PDE model, if the D_c estimation were high, then the predicted Ca^{2+} propagation velocities would also be elevated. To address this further, we used a second approach to the Ca^{2+} buffering by introducing two linear buffering coefficients β_l and β_c for the lumen and the cytosol, respectively. These coefficients are the fractional change in free $[Ca^{2+}]$ that results from any change in total $[Ca^{2+}]$. With $\beta_c = 0.06$ and $\beta_l = 0.12$ and the parameters given by the Fig. 1 legend, the experimentally-observed wave speed of 26 μm/s was reproduced. The wavelength (λ) of a spiral wave generated with these parameters (300 μm) was greater than was experimentally observed. More accurate representations of Ca^{2+} buffering and the kinetics of Ca^{2+} release and sequestration will be necessary to quantitatively model this phenomena.

In summary, we have mathematically formulated and numerically simulated a possible mechanism that may underlie the excitable properties of Ca^{2+} mobilization in *Xenopus* oocytes. Mathematical models cannot prove a biological mechanism. However, they are important for testing hypothesis and placing new experimental data in a known and testable framework.

APPENDIX

Here we show how the ordinary differential equations for the CICR model with no diffusion describe an excitable system of generic form. A typical and well studied excitable system is the FitzHugh-Nagumo (FHN) system, which was formulated as an approximation to the Hodgkin-Huxley theory of impulse propagation in neurons. The behavior of this model with no diffusion is analogous to the behavior of the space-clamped FHN equations and a detailed understanding of the excitable and oscillatory behavior of the CICR model may be obtained by analogy with the FHN equations.

The ODE representation of the CICR model (Eqs. 1 and 2 in the text) can be written as

$$\frac{dc}{dt} = \nu_o - K_{leak}c - \bar{f}(c, l) \tag{A1}$$

$$\frac{dl}{dt} = \bar{f}(c, l) \tag{A2}$$

$$\bar{f}(c, l) = V_p\left(\frac{c^2}{c^2 + K_p^2}\right) - V_m\left(\frac{c^4}{c^4 + Kc^4}\right)\left(\frac{l^2}{l^2 + K_l^2}\right) - K_{ER}l, \tag{A3}$$

where $\bar{f}$ (the exchange function) governs the dynamics of Ca^{2+} exchange between the cytoplasm and the IP_3-insensitive pool, and ν_o governs the rate of Ca^{2+} release into the cytoplasm from the IP_3-sensitive pool. We therefore treat ν_o as the bifurcation parameter, dependent on the level of agonist stimulation. In fact, Eqs. A1 and A2 describe a family of models of a particular structure; the analysis is the same for a wide range of exchange functions.

For convenience, we nondimensionalize Eqs. A1–A3. We set $z = c/K_p$, $y = l/K_l$, $\tau = tK_{leak}$, $\alpha = K_c/K_p$, $\beta = V_p/V_m$, $\gamma = K_l/K_p$, $\delta = K_{er}K_l/V_m$, $\mu = \nu_o/(K_{leak}K_p)$, $\epsilon = K_{leak}K_l/V_m$ to get

$$\frac{dz}{d\tau} = \mu - z - \frac{\gamma}{\epsilon}f(z, y) \tag{A4}$$

$$\frac{dy}{d\tau} = \frac{1}{\epsilon}f(z, y) \tag{A5}$$

$$f(z, y) = \beta\left(\frac{z^2}{z^2 + 1}\right) - \left(\frac{z^4}{z^4 + \alpha^4}\right)\left(\frac{y^2}{y^2 + 1}\right) - \delta y. \tag{A6}$$

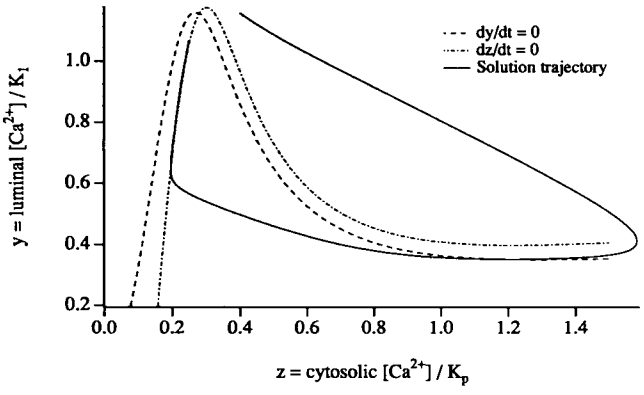

FIGURE A1 Nullclines of Eqs. A4–A6 and a typical solution trajectory. Except $\nu_o = 2.8$, the same parameters and initial conditions as in Fig. 4 *B* were used.

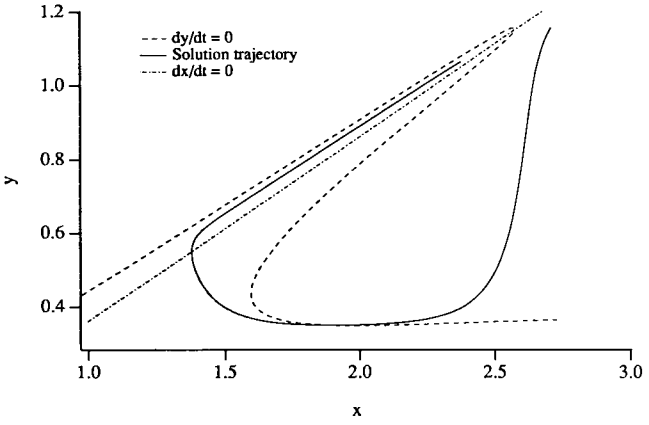

FIGURE A2 Nullclines of Eqs. A7 and A8 and a typical solution trajectory. The parameters and solution trajectory are the same as in Fig. A1. Note the "N-shaped" $dy/dt = 0$ nullcline and the linear $dx/dt = 0$ nullcline. From the shape of these nullclines we may obtain a qualitative understanding of the behavior of the Goldbeter et al. model by analogy with other well studied systems such as the FitzHugh-Nagumo equations.

Note that if the kinetics of the exchange of Ca^{2+} between the cytoplasm and the IP_3- insensitive pool is fast (i.e., V_m and V_p are large), ϵ will be a small parameter. For the values used in this paper, $\epsilon \approx 0.04$. The nullclines and a typical solution trajectory are shown in Fig. A1.

In Eqs. A4 and A5, the fast and slow time scales are not distinct (as in the FHN system) because the variable z is both a fast and a slow variable. However, this can be remedied. Let $x = z + \gamma y$ to get

$$\frac{dx}{d\tau} = \mu - (x - \gamma y) \tag{A7}$$

$$\frac{dy}{d\tau} = \frac{1}{\epsilon}f(x - \gamma y, y) = \frac{1}{\epsilon}F(x, y). \tag{A8}$$

In Eqs. A7 and A8, x is a slow variable and y is a fast variable. The nullclines and the same trajectory as in Fig. A1 are shown in Fig. A2.

It is clear from Fig. A2 that the nullclines of this model consist of a straight line and an N-shaped curve, and are qualitatively the same as the nullclines in the FHN system. As these are the nullclines of a generic excitable system, much of the detailed behavior of the model (the presence of a threshold, excitability, refractory states, the development of oscillations) may be understood within this general framework.

We gratefully acknowledge Christyne Bliton's assistance in confocal imaging. We also thank Jon Camp and all the support staff at the Biodynamics Research Unit for their expertise in image processing with the ANALYZE software.

The J. W. Kieckhefer Foundation supports S. Girard; the American Heart Association supports Dr. Lechleiter and Dr. Clapham; and the National Institutes of Health supports Dr. Clapham.

Received for publication 11 July 1991 and in final form 30 September 1991.

REFERENCES

1. Lechleiter J., S. Girard, E. Peralta and D. Clapham. 1991. Spiral calcium wave propagation and annihilation in *Xenopus laevis* oocytes. *Science (Wash. DC).* 252:123–126.
2. Berridge M. J., and R. F. Irvine. 1989. Inositol phosphates and cell signalling. *Nature (Lond.).* 341:197–205.
3. Tsunoda, Y. 1991. Oscillatory Ca^{2+} signalling and its cellular function. *New Biologist.* 3:1:3–17.
4. Berridge, M. J. 1990. Calcium oscillations. *J. Biol. Chem.* 265:17: 9583–9586.
5. Meyer, T., and L. Stryer. 1988. Molecular model for receptor-stimulated calcium spiking. *Proc. Natl. Acad. Sci. USA.* 85:5051–5055.
6. Goldbeter, A., G. Cupont, and M. J. Berridge. 1990. Minimal model for signal-induced Ca^{2+} oscillations and for their frequency encoding through protein phosphorylation. *Proc. Natl. Acad. Sci. USA.* 87:1461–1465.
7. Dupont, G., M. J. Berridge, and A. Goldbeter. 1991. Signal-induced Ca^{2+} oscillations: properties of a model based on Ca^{2+}-induced Ca^{2+} release. *Cell Calcium.* 12:73–85.
8. Finch, E. A., T. J. Turner, and S. M. Goldin. 1991. Calcium as a coagonist of inositol 1,4,5-trisphosphate-induced calcium release. *Science (Wash. DC).* 252:443–446.
9. Willcocks, A. L., B. V. L. Potter, A. M. Cooke, and S. R. Nahorski. 1988. Myo-inositol (1,4,5) trisphosphorothioate binds to specific [3H] inositol (1,4,5) trisphosphate sites in rat cerebellum and is resistant to 5-phosphatase. *Eur. J. Pharmacol.* 155:181–183.
10. Hamblin, M.R., J. S. Flora, and B. V. L. Potier. 1987. Myoinositol phosphorothioates, phosphatase-resistant analogues of myo-inositol phosphates. *Biochem. J.* 246:771–774.
11. Taylor, C. W., M. J. Berridge, K. D. Brown, A. M. Cooke, and B. V. L. Potter. 1988. DL-myo-inositol 1,4,5-trisphosphorothioate mobilizes intracellular calcium in Swiss 3T3 cells and *Xenopus* oocytes. *Biochem. Biophys. Res. Commun.* 150:626–632.
12. Berridge, M. J. 1987. Inositol trisphosphate and diacylglycerol: two interacting second messengers. *Annu. Rev. Biochem.* 56:159–193.
13. Backx, P. H., P. P. DeTombe, J. H. K. VanDeen, B. J. M. Mulder, and H. E. D. J. TerKeurs. 1989. A model of propagating calcium-induced calcium release mediated by calcium diffusion. *J. Gen. Phys.* 93:5:963–978.
14. Whitaker, M., and R. F. Irvine. 1984. Inositol 1,4,5-trisphosphate microinjection activates sea urchin eggs. *Nature (Lond.).* 312:636.
15. Irving, M., J. Maylie, N. L. Sizto, and W. K. Chandler. 1990. Intracellular diffusion in the presence of mobile buffers: application to proton movement in muscle. *Biophys. J.* 57:717–721.
16. Kuba, K., and S. Takeshita. 1981. Simulation of intracellular Ca^{2+} oscillation in a sympathetic neurone. *J. Theor. Biol.* 93:1009–1031.
17. Winfree, A. T. 1990. Vortices in motionless media. *Appl. Mech. Rev.* 43:297–309.
18. Bird, R. B., W. E. Stewart, and E. N. Lightfoot. 1960. Transport Phenomena. John Wiley & Sons, New York. 780 pp.
19. Press, W. H., B. P. Flannery, S. A. Teukolsky, and W. T. Vetterling. 1988. Numerical Recipes in C. Cambridge University Press, New York. 735 pp.
20. Britton, N. F. 1986. Reaction Diffusion Equations and Their Application to Biology. Academic Press, New York. 277 pp.
21. Murray, J. D. 1989. Mathematical Biology. Springer Verlag, New York. 767 pp.
22. Jahnke, W., W. E. Skaggs, and A. T. Winfree. 1989. Chemical vortex dynamics in the Belousov-Zhabotinsky reaction and in the two-variable Oregonator model. *J. Phys. Chem.* 93:740–749.
23. Markus, M., and B. Hess. 1990. Isotropic cellular automaton for modelling excitable media. *Nature (Lond.).* 347:56–58.
24. Gerhardt, M., H. Schuster, and J. J. Tyson. 1990. A cellular automaton model of excitable media including curvature and dispersion. *Science (Wash. DC).* 247:1563–1566.
25. Connor, J. A., and G. Nikolakopoulou. 1982. Calcium diffusion and buffering in nerve cytoplasm. *Lect. Math. Life Sci.* 15:79–101.
26. Crank, J. 1975. The Mathematics of Diffusion. 2nd ed. Clarendon Press, Oxford. 414 pp.